Korea-Australia Rheology Journal
Vol. 21, No. 4, December 2009 pp. 213-223

The effects of drag reducing polymers on flow stability : Insights from the Taylor-Couette problem

Cari S. Dutcher and Susan J. Muller*
Department of Chemical Engineering, University of California, Berkeley Berkeley, CA 94720-1462, U.S.A.
(Received May 13, 2009)

Abstract

Taylor-Couette flow (*i.e.*, flow between concentric, rotating cylinders) has long served as a paradigm for studies of hydrodynamic stability. For Newtonian fluids, the rich cascade of transitions from laminar, Couette flow to turbulent flow occurs through a set of well-characterized flow states (Taylor Vortex Flow, wavy Taylor vortices, modulated wavy vortices, *etc.*) that depend on the Reynolds numbers of both the inner and outer cylinders (Re_i and Re_o). While extensive work has been done on (a) the effects of weak viscoelasticity on the first few transitions for $Re_o=0$ and (b) the effects of strong viscoelasticity in the limit of vanishing inertia (Re_i and Re_o both vanishing), the viscoelastic Taylor-Couette problem presents an enormous parameter space, much of which remains completely unexplored. Here we describe our recent experimental efforts to examine the effects of drag reducing polymers on the complete range of flow states observed in the Taylor-Couette problem. Of particular importance in the present work is 1) the rheological characterization of the test solutions via both shear and extensional (CaBER) rheometry, 2) the wide range of parameters examined, including Re_i, Re_o, and Elasticity number El, and 3) the use of a consistent, conservative protocol for accessing flow states. We hope that by examining the stability changes for each flow state, we may gain insights into the importance of particular coherent structures in drag reduction, identify simple ways of screening new drag reducing additives, and improve our understanding of the mechanism of drag reduction.

Keywords : instabilities, Taylor-Couette, drag reduction, elastic turbulence

1. Introduction

The Taylor-Couette (TC) problem, which consists of flow in the annular gap between concentric, rotating cylinders, has long been a paradigm for studies of nonlinear dynamics and hydrodynamic stability for both Newtonian and non-Newtonian fluids. Even for the Newtonian case, the TC problem presents both a huge parameter space to explore and a rich cascade of flow transitions from the base flow to featureless turbulence through flow states of increasing complexity. The presence of many different flow states which vary in spatial and temporal symmetry is of special interest in the present study, since it permits examination of the effect of polymers on each of the flow states. We anticipate that by examining the effect of drag reducing polymers on these varied, isolated flow states and features, we will gain insight into the polymer-induced turbulence suppression associated with drag reduction in pipe flow; in pipe flow, the single, catastrophic transition from laminar to turbulent flow obscures the impact of the polymer on specific flow features. We hope that by examining the stability changes for each flow state in TC flow, we may gain insights into the importance of particular coherent structures in drag reduction, identify simple ways of screening new drag reducing additives, and improve our understanding of the mechanism of drag reduction.

In terms of the parameter space, the TC geometry is parameterized by a radius ratio $\eta = R_i/R_o$, where R_i is the radius of the inner cylinder and R_o is the radius of the outer cylinder, and an aspect ratio $\Gamma = h/d$, where h is the cylinder height and d is the gap between the cylinders ($d = R_o - R_i$). For Newtonian fluids, for a particular η and Γ, the flow state observed is determined by two Reynolds numbers, one based on the inner cylinder angular velocity Ω_i and one based on outer cylinder angular velocity Ω_o, and – for at least the higher flow states – the method by which the final conditions are reached. Here, we define the Reynolds numbers as $Re_i = \Omega_i R_i d/\nu$ and $Re_o = \Omega_o R_o d/\nu$, respectively, where ν is the kinematic viscosity. We refer to the method by which the final Re_i and Re_o are reached as the ramping protocol, which we discuss below. The critical condition defining the onset of a particular flow state, Re_c, a critical Reynolds number based on Re_i, is thus a function of η, Γ, Re_o, and, potentially, ramping protocol.

The complexity of the system is suggested by consid-

*Corresponding author: muller2@berkeley.edu

ering the Newtonian problem with a stationary outer cylinder, *i.e.*, $Re_o=0$, and quasi-static ramping protocol. Here, the purely azimuthal base flow (AZI) observed at low Re_i undergoes a primary transition to stationary, axisymmetric toroidal vortices (Taylor Vortex Flow, TVF) at a critical Re_i. TVF is replaced, at higher Re_i, by time-dependent, non-axisymmetric vortices characterized by a single temporal frequency (wavy vortex flow, WVF), and subsequently by non-axisymmetric vortices with multiple temporal frequencies (modulated wavy vortex flow, MWV). At still higher Re_i, the flow undergoes a series of transitions to weakly turbulent states, with coherent structures and multiple distinct temporal frequencies present (chaotic wavy vortex flow, CWV), a single distinct temporal frequency (wavy turbulent vortex flow, WTV), and finally no distinct temporal frequency (turbulent Taylor vortex flow, TTV).

When the outer cylinder is also rotated, so that $Re_o \neq 0$, a broad spectrum of additional flow states are accessible and the pathway to turbulence varies. Re_c for the primary transition from AZI is insensitive to aspect ratio Γ for $\Gamma > 10$ (Walden and Donnelly, 1979; Cole, 1976), and analytic expressions (Esser and Grossmann, 1996) and dynamic parameterization using phenomenological scaling (Coles, 1967; Dutcher and Muller, 2007) have been developed to describe $Re_c(\eta, Re_o)$. However, unlike the first transition, the critical conditions for higher flow states are sensitive to and no formulas or descriptions for these $Re_c(\eta, \Gamma, Re_o)$ exist. The stability boundaries in the $Re_i - Re_o$ plane, including the flow states above plus many others, for a TC cell with $\eta = 0.883$ and $20 < \Gamma < 48$ and a quasi-static ramping protocol were determined experimentally in a seminal study by Andereck *et al.*(1986). Reviews of the Newtonian TC problem have been published by Koschmieder (1993), Di Prima and Swinney (1985), and Tagg (1994).

The non-Newtonian TC problem has received far less attention than the Newtonian problem, and very little is known about the higher order flow states and the effects of outer cylinder rotation ($Re_o \neq 0$) and ramping protocol in the viscoelastic case. Twin challenges complicate the non-Newtonian TC problem: 1) the complete rheological characterization of the non-Newtonian fluids in terms of their material coefficients (*e.g.*, the shear rate-dependent solution viscosity $\eta_T(\dot{\gamma})$, normal stress coefficients $\Psi_1(\dot{\gamma})$ and $\Psi_2(\dot{\gamma})$, relaxation time λ_p, *etc.*), and 2) the increased dimensionality of the TC parameter space, since critical conditions depend not only on η, Γ, Re_o and ramping protocol, but also on a host of dimensionless parameters based on these material coefficients.

Early experiments, by Rubin and Elata (1966), Giesekus (1966, 1972), Denn and co-workers (Denn and Roisman, 1969; Ginn and Denn, 1969) and others, focused on weakly elastic, dilute solutions, with $Re_o=0$. Giesekus, using varying concentrations of polyacrylamide, was the first to report both the non-monotonic effect of fluid elasticity (here, due to varying polymer concentration) on the critical condition for the primary transition from AZI flow and the appearance of new flow states due to elasticity, which he referred to as "oscillatory instabilities" and "elastic turbulence" (Giesekus, 1966). Others noted the importance of the second normal stress coefficient on the critical condition for the primary transition (Ginn and Denn, 1969), and the role of shear-thinning of the solution viscosity in determining the sequence of transitions with increasing Re_i (Haas and Buhler, 1989). Unfortunately in most of these early experiments, fluid rheological characterization was either entirely absent or incomplete (*e.g.*, in some cases, viscosity was measured as a function of shear rate, but no normal stress coefficient data were reported).

More recent experimental TC studies of non-Newtonian fluids in the limit of weak elasticity have parameterized elastic effects through the elasticity number, $El = \lambda_p/(d^2/\nu)$, which can be thought of as the ratio of a polymer time scale λ_p to a viscous time scale (or the ratio of a Deborah number to a Reynolds number). Yi and Kim (1997), using $Re_o = 0$, examined very dilute solutions of polyacrylamide, xanthan gum, and polyacrylic acid, and found the same series of transitions as for Newtonian fluids for all solutions; the critical condition for the onset of TVF increased with polymer concentration for all polymers. Baumert and Muller (1995; 1997a,b; 1999) examined transitions in non-shear-thinning, dilute viscoelastic solutions of polyisobutylene (Boger fluids) at El values of 0.16 and 44, (achieved by varying the solvent viscosity) for flows with both zero and non-zero values of Re_o. These authors documented a number of new flow states, including axially traveling vortices and a disordered, oscillating "flame pattern"; however, as with many of the earlier studies, flow states were generated through rapid ramps in Re_i rather than through a consistent, quasi-static ramping protocol. Groisman and Steinberg (1996; 1997; 1998) using shear-thinning polyacrylamide solutions and considering only $Re_o=0$, were able to vary El over three decades (from roughly $0.02 < El < 20$) by varying temperature and solvent composition. These authors explored the Re_i – El plane via abrupt steps in Re_i (rather than quasi-static ramps) and found transitions from AZI to TVF to a rotating standing wave state (RSW) to disordered oscillations (DO, a state characterized by chaotic changes in radial and axial velocities) at $El < 0.2$. In this limit of $El < 0.2$, the critical condition for TVF was essentially independent of El. At modestly higher El, AZI flow transitions directly to disordered oscillations, and the critical condition Re_c decreased with increasing El. Crumeyrolle *et al.* (2002), in experiments with $Re_o=0$ and an unspecified ramping protocol, varied El by changing the concentration of polyethylene oxide (PEO) in de-ionized water. They also reported different transitions above a critical El value; for $El < 0.06$

AZI becomes unstable to TVF followed by WVF (*i.e.*, the same first two transitions as in Newtonian TC flows); for El>0.06 AZI transitions directly to rotating standing waves (RSW). Increasing El destabilized AZI for all values of El probed. Crumeyrolle *et al.* attribute the change in pathway at least in part to the onset of shear-thinning at the higher polymer concentrations needed to achieve higher El values, although the ratio of the polymeric to solvent contributions to the solution viscosity were also varying with El in their study.

Recent numerical studies by Thomas *et al.* (2006; 2009) have succeeded in predicting some of the features of the experiments described above. Using a FENE-P constitutive model, and fluid and geometric parameters comparable to those used in experiments, the authors performed three-dimensional, time-dependent simulations of Taylor-Couette flow with $Re_o=0$. For El=1/3, they find that when the inner cylinder rotation speed is raised above the linear stability threshold, AZI flow becomes unstable to RSW, followed, at increasing Re_i, by modulated RSW, oscillatory strips (OS, similar to Baumert and Muller's flame pattern), and then disordered oscillations. On decreasing Re_i, the chaotic, disordered oscillations decay to time-dependent OS or stationary, axisymmetric diwhirls (DW). Thomas *et al.* (2009) find that the presence of localized, solitary vortex structures such as OS and DW is a common feature of these flows, even at El>1.

The studies above, with different polymers and different ways of varying El, suggest the vastness of the parameter space in the non-Newtonian Taylor-Couette problem. Many rheological parameters differ across existing experiments, and relatively subtle differences in rheological behavior (*i.e.*, small changes in shear-thinning, the ratio of polymeric to solvent contributions to the total solution viscosity, Ψ_2, El, chain stiffness) can lead to large stability changes. More comprehensive reviews of the non-Newtonian Taylor-Couette problem, including studies in the high elasticity (E>>1) limit, may be found in the references by Petrie and Denn (1976), Larson (1992), Shaqfeh (1996), and Muller (2008).

In the present study, we extend existing experimental results on the effects of weak elasticity on the Taylor-Couette problem using our custom-built, computer-controlled, high aspect ratio Taylor-Couette cell. We have experimentally examined Newtonian fluids and a series PEO solutions of varying elasticity. Our work is distinguished by the use of both shear and capillary break-up extensional rheometry (CaBER) to characterize the test fluids, the use of a consistent and conservative ramping protocol for reaching each flow state, and through our systematic investigation of large regions of the Re_i – Re_o plane for each solution, including weakly turbulent flow states at high Re_i. Since we are varying Elasticity number by varying polymer concentration, polymer molecular weight, and solvent composition, we have essentially mapped the three dimensional Re_i – Re_o – El space suggested by Fig. 1. In addition, since we are accessing higher order transitions and flow states that vary in spatial and temporal symmetry, we anticipate that the effects of elasticity will vary with the flow state. By examining which flow states are stabilized or destabilized by the presence of polymer, we hope to provide insights into the role of particular coherent structures in drag reduction, and suggest ways of screening potential drag reducing agents.

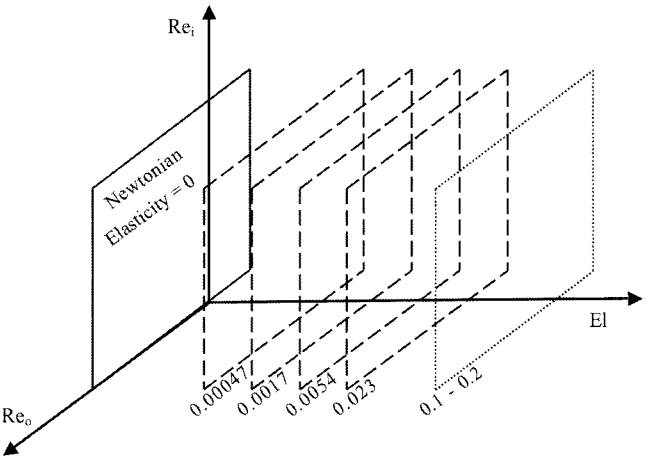

Fig. 1. The parameter space examined in the present study. Taylor-Couette flow stability in six planes of Re_i–Re_o with El =0, 0.00047, 0.0017, 0.0054, 0.023, and~0.2 have been mapped.

2. Experimental Methods

All of our experiments were conducted in a custom designed and built Taylor-Couette cell with inner and outer cylinder radii of $R_i=0.06946$ m and $R_o=0.07615$ m and cylinder height h=0.406 m, corresponding to a radius ratio $\eta=0.912$ and an aspect ratio $\Gamma=60.7$. The two cylinders may be rotated independently, and their motion is under computer control, as is the temperature of the TC cell. Test fluids were seeded with small concentrations of anisotropic tracers (mica flakes) and the flow was visualized in either the r-z plane by illuminating the gap between the cylinders with a sheet of laser light or in the z-projected-θ plane by illuminating the entire cell with ambient lighting. As discussed below, critical conditions and flow states were accessed (except for the highest turbulent transitions of turbulent Taylor vortex flow (El=0, 0.00047) or modulated turbulence (El=0.0017)) via quasi-static ramps in Re_i. Flow visualization movies of the flow evolution with time (or equivalently, Re_i) in the r-z and z-θ planes were captured with CCD cameras, and processed to produce space-time plots (or space-Re_i plots). 2-D FFTs were then taken of small, overlapping regions of the space-time plots to

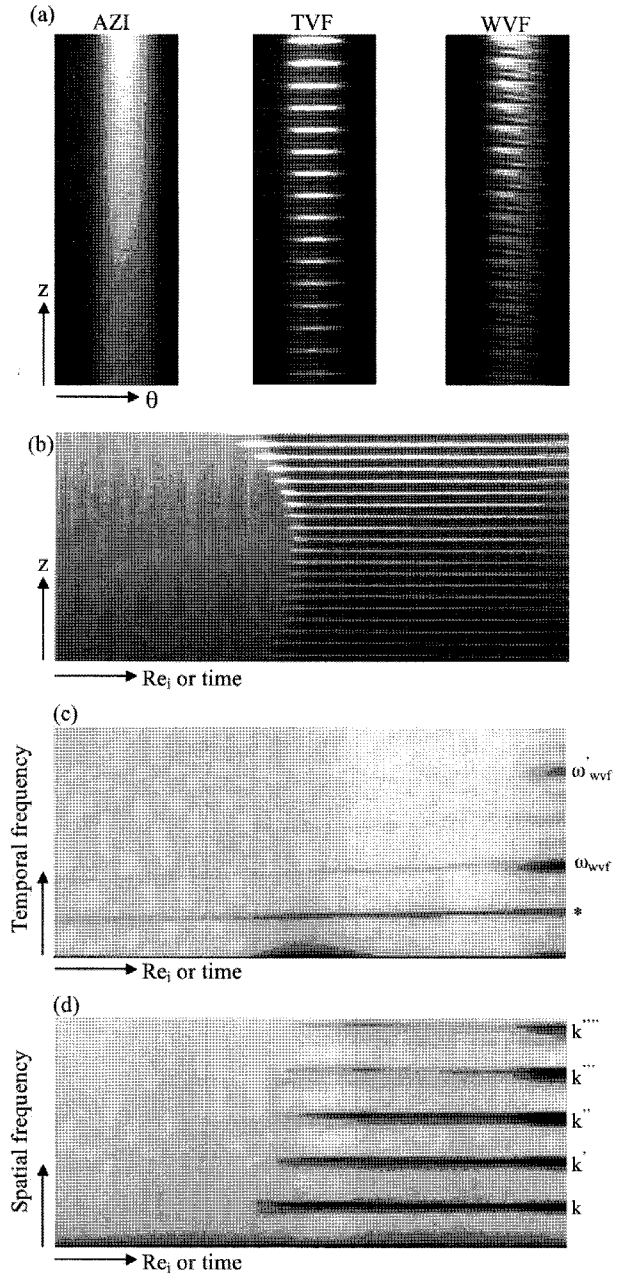

Fig. 2. Set of sample ambient images from a movie at El = 0.023 and $Re_o = 0$ of the (z-θ) plane showing azimuthal flow (AZI), Taylor vortex flow (TVF), and wavy vortex flow (WVF) at $Re_i = 134.8$, 163.1, and 174.7, respectively (a). Space-time plot formed from the same experiment from $134.8 < Re_i < 174.1$ (b). Temporal (c) and Spatial (d) frequency-time plots, where harmonics of the distinct temporal (ω_{WVF}) and spatial (k, associated with TVF) frequencies are denoted with an apostrophe (') and a peak due to cylinder rotation is marked with an asterisk (*).

produce frequency-time plots. These frequency-time plots show the magnitude of the complex modulus of the FFT as a function of either temporal frequency or spatial frequency k as a function of time (*i.e.*, , $<|F(\omega)|>_k$ versus time t or $<|F(k)|>_\omega$ versus t). From these frequency-time plots, then, we can identify the critical conditions from the appearance or disappearance of particular temporal or spatial modes.

Fig. 2(a) contains a set of sample ambient images from a movie at El = 0.023 and $Re_o = 0$ of the (z-θ) plane showing azimuthal flow (AZI), Taylor vortex flow (TVF), and wavy vortex flow (WVF) at $Re_i = 134.8$, 163.1, and 174.7, respectively. Fig. 2(b) shows the space-time plot formed from the same experiment from $134.8 < Re_i < 174.1$, and Fig. 2(c) and 2(d) show the two frequency-time plots (temporal and spatial) that correspond to the space-time plot in Fig. 2(b). Harmonics of the distinct temporal (ω_{WVF}) and spatial (k, associated with TVF) frequencies are denoted with an apostrophe ('). Note that due to non-uniformities in the anodization of the inner cylinder, a peak appears due to cylinder rotation even in purely azimuthal flow. This peak, marked with an asterisk (*) in Fig. 2(c), is not associated with the flow state. Further details regarding the TC apparatus, cylinder motion control, temperature control (±0.1°C), mica flake concentrations, image capture and processing, and Compumotor and National Instruments platforms used for automation of the experiments can be found in the references by Dutcher, White, and Muller (Dutcher, 2009; Dutcher and Muller, 2009a; White, 2002; White and Muller 2002a,b, 2003).

A series of Newtonian fluids of different viscosities η_T and consisting of varying concentrations of glycerin in water were used to first map the stability diagram (the $Re_i - Re_o$ plane at El = 0) for our apparatus. This step was necessary since our apparatus differs in radius ratio from that used by Andereck *et al.* (1986) in their classic study. The effects of elasticity, El, were then probed through a series of five solutions of high molecular weight PEO in glycerin/water solvents. Fluids were designed to allow access to high Reynolds numbers in our TC apparatus so that higher order transitions could be accessed. The compositions of these five solutions, their kinematic viscosities, and the polymeric relaxation time for each fluid are summarized in Table 1. For all PEO solutions, the polymeric relaxation times were determined using capillary break-up extensional rheometry (CaBER). Steady shear viscometry was also performed on all fluids and the four lowest elasticity fluids (PEO1-PEO4) were all found to be non-shear-thinning. The highest elasticity fluid (PEO5) was mildly shear-thinning (power-law index n = 0.88, where the viscosity has been fit to a power-law $\eta_T = k\dot{\gamma}^{n-1}$). For the Newtonian and non-shear-thinning PEO solutions (PEO1-PEO4), the kinematic viscosities in Table 1 were determined via capillary viscometry, while the kinematic viscosity of the moderately shear- thinning PEO5 was found as a function of shear rate using rotational rheometry and density measurements. PEO5 was also sufficiently elastic to allow characterization via small amplitude oscillatory

Table 1. Test fluids, relaxation times, and elasticity numbers

	PEO concentration (ppm)	PEO molecular weight (MDa)	Glycerin concentration in solvent (wt%)	kinematic viscosity, ν (mm^2/s)	λ polymer (ms)	El
Glycerin/water	0	-	various	various	0	0
PEO1	250	2	30	2.617	8.0	0.00047
PEO2	750	2	30	3.892	20	0.0017
PEO3	750	2	45	6.886	35	0.0054
PEO4	750	2	60	13.99	72	0.023
PEO5	850	5	47	17.21 to 8.444	550	0.21 to 0.1

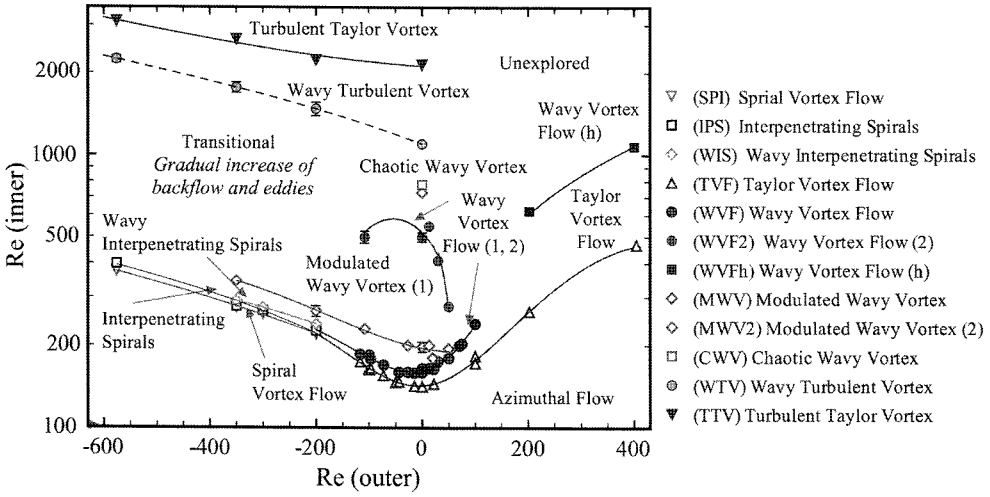

Fig. 3. Newtonian Taylor-Couette flow stability map for radius ratio 0.912 and aspect ratio 60.7. Dashed lines indicate a gradual transition boundary. High Re_i for the co-rotation space was not explored. Transitions with $Re_o < -50$ where determined through visual inspection of the fluid motion and space-time plots, instead of the detailed spectral analysis used to identify all other transitions.

shear (SAOS) and the relaxation time determined using SAOS was in good agreement with the CaBER value. Complete rheological characterization of the test fluids can be found in Dutcher (2009) and Dutcher and Muller (2009b).

As noted in the introduction, an important, distinguishing aspect of the present work is the use of a very consistent and conservative ramping protocol to access flow states. Use of very rapid ramps or large steps in Re_i can result in over-shooting the critical conditions and/or kicking the flow system into anomalous flow states. To determine an appropriately slow, quasi-static ramping rate, we measured the critical condition for the onset of TVF in Newtonian fluids via a series of ramps of decreasing dimensionless ramp rate, $dRe_i/d\tau$, where τ is time made dimensionless with the viscous time scale $(R_o-R_i)^2/\nu$. The rate below which the critical condition for TVF was found to be independent of ramp rate and equal to the linear stability prediction (within experimental error) was defined as the critical ramp rate $a_c = dRe_i/d\tau \leq 0.68$. This rate is consistent with the ramping protocol used by Andereck and co-workers (1986). Note that since the polymer relaxation time is much shorter than the viscous time scale, we anticipate that this rate will also be extremely conservative with respect to the development of elastically-influenced flow states. For the shear-thinning fluid, we note that we have dynamically controlled the ramping rate to account for the changing viscosity with shear rate. A more detailed description of the ramping protocol, and the determination of the critical ramp rate, is included in the reference by Dutcher and Muller (2009a).

3. Results & Discussion

3.1. Newtonian Results

In order to determine the effects of elasticity on the stability boundaries for the various flow states, we must first map the Re_i — Re_o plane for Newtonian fluids, since our apparatus differs in radius ratio η from those TC geometries for which complete stability maps have been pub-

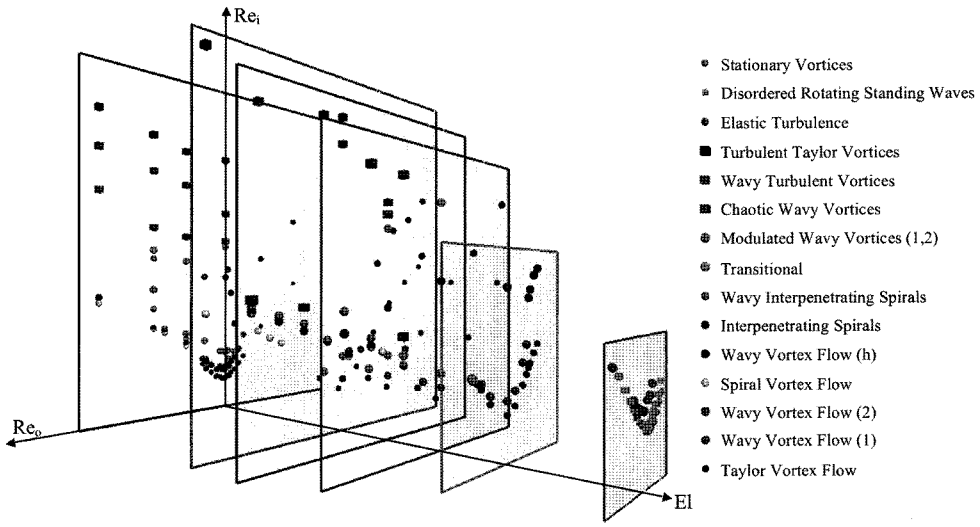

Fig. 4. 3D stability phase-space, including critical conditions for fifteen different flow states for Newtonian and non-Newtonian fluids for $0<El<1$. This plot is the completion of the 3D stability phase-space proposed in Fig. 1.

lished, and radius ratio is known to affect the stability boundaries. As noted above, while the non-monotonic effect of η on the *primary* transition (from AZI to either TVF or spirals, depending on Re_o) has been well-studied and expressions have been developed to describe $Re_c(\eta, Re_o)$ for this *first* transition (Esser and Grossmann, 1996; Coles, 1967; Dutcher and Muller, 2007), there is no such description for secondary and higher order flow states. Our results for the Newtonian plane for $\eta=0.912$, identifying 13 different flow states in the range of Re_i and Re_o accessed in our study, are shown in Fig. 3. A comparison of our results for $\eta=0.912$ to those of Andereck *et al.* (1986) for $\eta=0.883$ reveals that the effect of η on Re_c is, in general, non-monotonic and mode-dependent. That is, different modes (spirals, WVF, TTV, *etc.*) are affected differently by η. Fig. 3 thus forms the basis for our examination of the effects of elasticity on the various flow states accessed with our polymeric fluids. Note that while the stability boundaries for Re_o near zero and $Re_o>0$ were determined based on our Fourier transform analysis (*cf* above and Fig. 2(c)), stability boundaries for high counter-rotation ($Re_o<-50$) were determined simply from space-time plots (as in Fig. 2(b)) and are somewhat less precisely known. From here, only the precise, spectrally determined Newtonian critical conditions are used in the study of the effects of elasticity.

3.2. Low Elasticity Results ($0<El<0.023$)

The results for all the fluids are indicated schematically in Fig. 4. Critical conditions for thirteen different flow states are indicated on the five $Re_i - Re_o$ planes with $El > 0$. There are many ways to plot and examine the data; as with the effect of radius ratio on the critical conditions for different flow states, we find the effects of El are non-

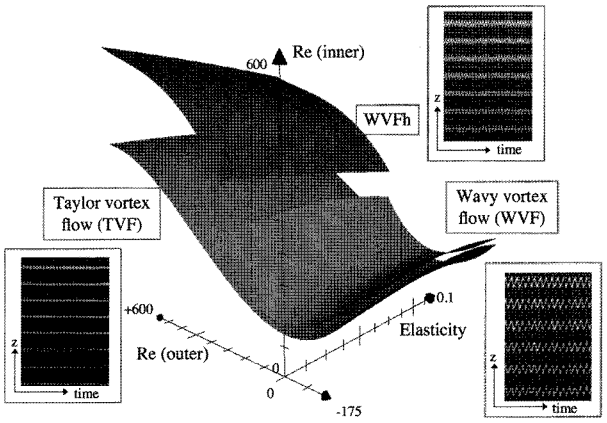

Fig. 5. El - Re_i - Re_o 3D phase plot for the envelope of stability of TVF between the primary (gray tones) and secondary transition surfaces (blue tones and red tones) for $-100<Re_o<500$ and $El\leq0.023$. The Newtonian Re_i - Re_o plane is plotted at vanishing El of 0.00001. The surface is a fit to the data points from a multiple parameter polynomial equation.

monotonic and mode-dependent. Here, we find it most useful to consider first the four lowest elasticity fluids (with $0<El\leq0.023$) prior to discussing the most elastic fluid ($El\sim0.2$) in the next section.

For all fluids with $El\leq0.023$, we find the *initial* transitions from the base azimuthal flow (AZI) with increasing Re_i are to the same flow states as are observed for Newtonian fluids. That is, the primary transition from azimuthal flow for $-175<Re_o<400$ is to Taylor Vortex Flow (TVF). The critical condition for the primary transition, Re_{c_TVF}, varies non-monotonically with El, but is only moderately affected by El, with Re_{c_TVF} at a given Re_o varying by roughly 15%. As in Newtonian fluids, the secondary transition from TVF is to wavy vortex flow (WVF) except at high co-rotation

($Re_o \geq 200$), where the secondary transition is to a higher frequency wavy vortex flow that we refer to as WVFh. (We note that Andereck and co-workers identify this mode as wavelets for Newtonian fluids.) Here again the effect of El on the critical conditions is non-monotonic but modest, with $Re_{c\_WVF(h)}$ varying by no more than 20% from the Newtonian value at the same Re_o. Surfaces showing the stability boundaries for these first two transitions have been fit to the data points in Fig. 4 and are shown in Fig. 5. Note that the axes have been rotated relative to Fig. 4 to provide a better view of the stability boundaries. Insets in Fig. 5 also show small sections of space-time plots for the three flow states: TVF, WVF, and WVFh. From Fig. 5, the effects of elasticity are evident but are clearly less than the effects of varying Re_o for the range of El and Re_o probed.

We focus on the $Re_o = 0$ plane to consider the effects of El on transitions to higher order states at increasing Re_i. For Newtonian fluids, the transition pathway from AZI to turbulent Taylor vortices (TTV) follows the sequence of flow states: AZI → TVF → WVF_1 → MWV_1 → WVF_2 → MWV_2 → CWV → WTV → TTV. At the lowest (non-zero) El considered, El=0.00047, the same lower-order and higher-order transitions are observed, with no additional flow states due to elasticity. The lowest level of elasticity results in some modifications of the critical conditions for each state, and the degree of stabilization or destabilization varies with the flow state. For example, the critical Re_i for TVF increases from $Re_{c\_TVF} = 144 \pm 4.2$ for Newtonian fluids to $Re_{c\_TVF} = 153.8 \pm 1.94$ for El=0.00047. More significant modification is observed for higher-order flow states; for TTV, the critical conditions change from $Re_{c\_TTV} = 2150$ for El = 0 to $Re_{c\_TTV} \approx 2600$ for this lowest level of elasticity.

The next slight increase in El, to El=0.0017, results in the same transition pathway through WTV flow, but TTV was not observed even though Re_i considerably above that required to produce TTV in the lowest elasticity fluid were accessed. Instead, a modulated WTV flow state was observed near $Re_i \sim 2800$, in which the wavy turbulent structure associated with WTV is still evident, but the axial periodicity becomes less coherent and the temporal frequency spectrum shows broadening and modulation. This modulated turbulent state appears in place of TTV even to the upper limit of Re_i accessible ($Re_i \sim 3400$) which is approximately 1.6 times Re_{c_TTV} for Newtonian fluids. Details of this modulated turbulent state can be found in Dutcher (2009), and Dutcher and Muller (2009b). For this fluid, WVF_2 also appears to be significantly stabilized relative to the Newtonian case.

With an increase in El from 0.0017 to 0.0054, no transition to TTV was observed, although Re_i in excess of those required for the transition to TTV in Newtonian fluids could not be accessed due to experimental constraints. For this fluid, the transition pathway from AZI through WVF_2 remains similar to the Newtonian case (again, with shifts in the critical conditions that are mode-dependent), but now flow states beyond WVF_2 appear to be modified by the presence of elasticity. The onset of CWV, which is sudden and obvious in Newtonian fluids and for elasticity numbers of 0.00047 and 0.0017, now occurs gradually over a range of Re_i in the presence of multiple dominant temporal frequencies. Thus, at the lowest levels of elasticity only the critical conditions are modified but the flow states remain the same as in the Newtonian case. With increasing elasticity, we find that in addition to modifications of the critical conditions, higher order flow states are modified, with more flow states affected as elasticity increases.

3.3. High Elasticity Results (El~0.2)

To reach the highest level of elasticity probed in this study, a higher molecular weight PEO polymer (5 MDa versus 2 MDa) at a slightly higher concentration was used in solution PEO5 relative to the four lower elasticity fluids discussed above (*cf* Table 1). This fluid allows access to elasticity levels roughly an order of magnitude higher than the next most elastic fluid, but also displays some modest shear-thinning, resulting in the elasticity numbers accessed spanning a range from $0.10 < El < 0.21$. In the following, however, we refer to this as simply El~0.2.

For El~0.2 and $Re_o = 0$, the first transition from AZI flow is to stationary, axisymmetric vortices (SV) that appear similar to TVF in terms of axial wavenumber, but the vortices (which, as with TVF, fill the gap between the two cylinders) appear modified in form by elasticity. The vortices are squarer in cross-section than Taylor vortices and display broader inflow and outflow boundaries than TVF. The critical condition for this first transition is only modestly higher than the transition to TVF at El=0. More dramatic changes in the flow states are observed as Re_i is increased beyond the primary transition. The secondary transition from SV is to a rotating standing wave state characterized by slight axial disorder (DRSW) rather than to WVF. The critical condition, $Re_{c\_DRSW} \approx 162$, is again only slightly different from the critical condition for the onset of WVF for the next most elastic fluid (El = 0.023), $Re_{c\_WVF} \approx 171$, but the two flow states are clearly different, as shown in the space-time plots extracted from similar regions of the (z,θ) plane in Fig. 6. A direct comparison of Fourier transforms of the two space-time plots reveals broader spatial frequency peaks for DRSW and a small, broad temporal frequency peak at a lower temporal frequency (relative to the inner cylinder rotation frequency) rather than sharp, distinct peaks as in WVF. This DRSW state is similar to some of the standing wave states reported by Crumeyrolle *et al.* (2002) and Groisman and Steinberg (1996, 1997, 1998).

The most profound change due to higher El occurs with the next transition, where the DRSW state is replaced by

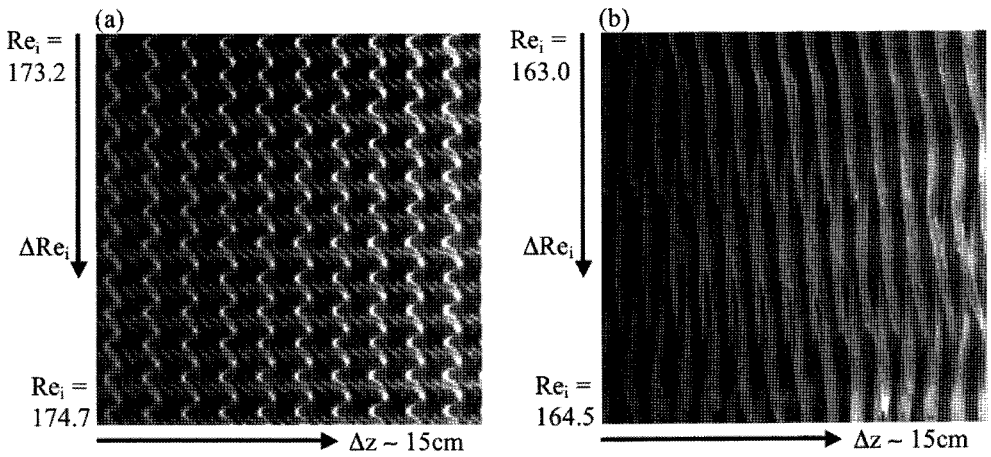

Fig. 6. Space-time plots extracted from the (z,) plane showing WVF for El=0.023 (a) and DRSW for El~0.2 (b). These are the flow states resulting from the secondary transition from TVF to WVF for El=0.023 and from SV to DRSW for El~0.2.

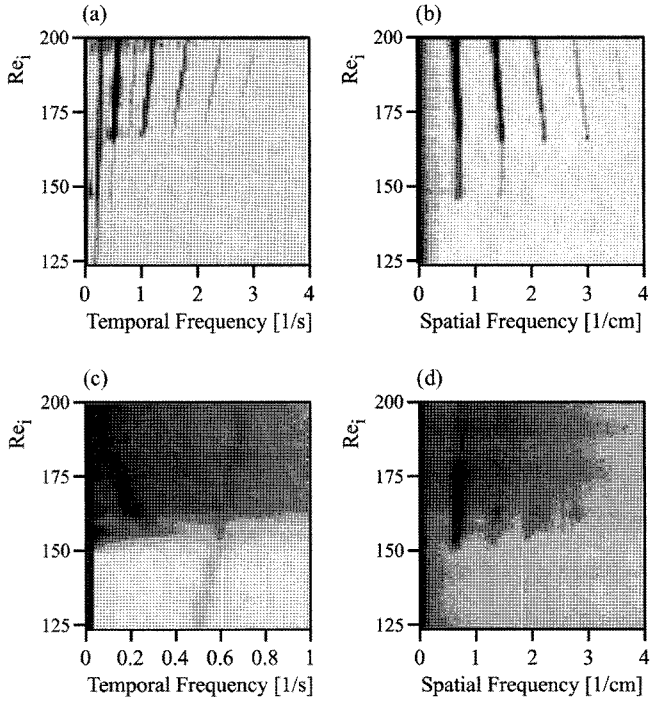

Fig. 7. Temporal and spatial frequency-time plots for Newtonian (a,b) and El 0.2 (c,d), respectively. All plots range over $123<Re_i<200$ with $Re_o=0$ and a quasi-static ramping protocol. The gray-scale represents the magnitude of the complex FFT, F, normalized by the maximum value (Max[F]) at each value of Re_i.

elastic turbulence (ET), a state characterized by very broad temporal and spatial power spectra, at $Re_{c\_ET} \approx 181$. The striking, qualitative differences in the early transitions between this highest elasticity fluid and all of the other fluids (PEO1 through PEO4 as well as the Newtonian fluids) are shown by the comparison of the frequency-time plots in Fig. 7. While the early transitions for Newtonian and low El fluids are marked by the appearance or disappearance of single, distinct spatial or temporal frequencies (accompanied at higher Re_i by higher harmonics), for El~0.2, the frequency-time plots reveal that fluid motion on a broad range of temporal and spatial scales occurs almost from the primary transition.

When the quasi-static ramp was performed from high Re_i to low Re_i (rather than the reverse), hysteresis in the flow states and transition pathway occurred for this highest El fluid. Whereas the transition pathway on increasing Re_i is AZI→SV→DRSW→ET, on *decreasing* Re_i, the transition pathway is ET→DRSW→ordered rotating standing waves→standing waves→AZI. No such pathway hysteresis was observed for any of the lower elasticity fluids. The ordered rotating standing wave and standing wave patterns are discussed more fully in Dutcher (2009).

Groisman and Steinberg (1996, 1997, 1998) have also reported hysteresis (using non-quasi-static ramps in Re_i) for elasticity numbers above approximately 0.2. They report a strongly hysteretic transition from AZI→ disordered oscillations (DO, a flow state similar to ET, but with strong, chaotically oscillating vortices, often with patches of standing and traveling waves) with increasing Re_i but observe oscillatory strips (OS) and stationary vortices or diwhirls prior to AZI following an abrupt decrease in Re_i. Thomas *et al.* (2009), in their numerical simulations, also report hysteresis at El=1/3. These authors report AZI→RSW→modulated RSW→OS→DO with increasing Re_i and DO→OS→diwhirls→AZI on decreasing Re_i. Thus, hysteresis in the transition pathway appears to be a general feature for El near 0.2.

Finally, we consider the effects of co- and counter-rotation ($Re_o \neq 0$) on transitions for the El~0.2 fluid. We observe elastic stabilization of AZI for counter-rotation and moderate co-rotation. The stabilization increases monotonically with increasing counter-rotation and results in about a 20% increase in the critical Re_i for $Re_o=-100$ (*cf*

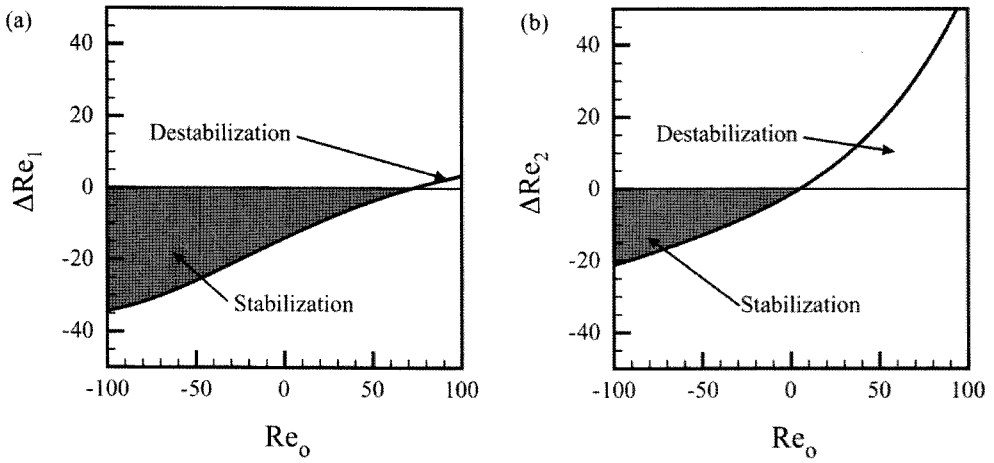

Fig. 8. Comparison of the elastic stabilization for the primary instability (a) and secondary instability (b) for a range of $-100 < Re_o < 100$. The curve ΔRe_1 in (a) was calculated by subtracting the critical condition for SV with El ~ 0.2 from the critical condition for TVF with El = 0 (*i.e.*, $\Delta Re_1 = Re_{c\_TVF}(El=0) - Re_{c\_SV}(El=0.2)$). The curve ΔRe_2 in (b) was calculated by subtracting the critical condition for DRSW with El ~ 0.2 from the critical condition for WVF with El = 0 (*i.e.*, $\Delta Re_2 = Re_{c\_WVF}(El=0) - Re_{c\_DRSW}(El=0.2)$). The margins of stability were generated by polynomial fits to experimental data. The dark gray regions are areas of elastic stabilization (*i.e.*, suppression of the primary (a) or secondary (b) instability to higher Re_i, while the light gray regions are areas of elastic destabilization (*i.e.*, enhances the onset of the primary or secondary instability).

Fig. 8(a)). For $Re_o > 70$, El ~ 0.2 results in slight destabilization of the azimuthal base flow; at $Re_o = 100$, Re_c for the primary transition decreases ~5%. Similar trends are observed for the secondary transition: counter rotation results in stabilization and co-rotation results in destabilization (Fig. 8(b)). However, in general, there is a larger region of destabilization of TVF in Fig. 8(b) than seen for AZI in Fig. 8(a). In addition, we find that the transition pathway becomes more elastically-influenced with increasing counter-rotation. For $-100 \le Re_o \le 150$, the transition pathway is AZI → SV → DRSW → ET, as discussed above. For moderate counter-rotation ($-180 \le Re_o \le -100$), the Taylor vortex-like flow state of SV vanishes, and AZI → DRSW → ET. At $Re_o = -225$, DRSW no longer appear, and azimuthal flow transitions directly to elastic turbulence, *i.e.*, AZI → ET, at $Re_{c\_ET} \approx 260$.

4. Conclusions

We have experimentally explored the effects of the drag-reducing polymer PEO on hydrodynamic transitions in the Taylor-Couette problem. Using a series of five solutions with varying elasticity, we have systematically investigated the effects of Re_i, Re_o, and El on the cascade of flow states observed. We have used a consistent, quasi-static ramping protocol to access flow states, and explored large regions of the three dimensional $Re_i - Re_o -$ El space suggested by Fig. 1. For the four solutions with El < 0.1, we find that the initial transitions are to flow states that are essentially identical in form to the flow states observed with Newtonian fluids. The critical conditions are modified by elasticity, however, and the effects of El on Re_c are non-monotonic

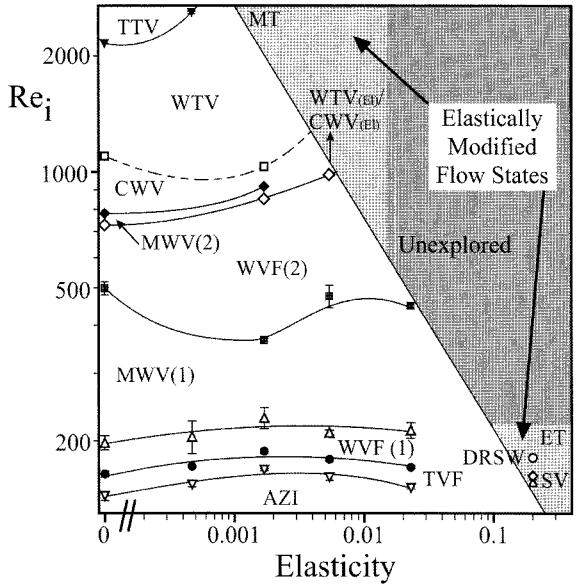

Fig. 9. El - Re_i stability plane for $Re_o = 0$. The flow states mapped include azimuthal flow (AZI), Taylor vortex flow (TVF), wavy vortex flow (WVF), modulated wavy vortex flow (MWV), chaotic wavy vortices (CWV), wavy turbulent vortices (WTV), turbulent Taylor vortices (TTV), modulated turbulence (MT), elastically modified chaotic or wavy turbulent vortices (WTV(El)/CWV(El)) stationary vortices (SV), disordered rotating standing waves (DRSW), and elastic turbulence (ET). Light gray regions indicate where elasticity modifies the flow states; dark gray regions were not explored in the present study.

and mode-dependent. With increasing El, modifications to the flow structure occur, with higher-order flow states

modified at lower levels of elasticity, and changes to lower-order flow states occurring at higher levels of elasticity. For the $Re_o=0$ plane, these effects are summarized in Fig. 9, where the shaded region shows the increasing influence of elasticity on lower Re_i transitions. For the most elastic fluid with $El\sim0.2$, even Taylor vortex flow is somewhat modified, and the frequency-time plots reveal the dramatic broadening of the temporal and spatial spectra following the primary transition. Hysteresis in the flow states is also observed at this highest elasticity number, and the effects of elasticity are heightened by increasing counter-rotation.

Acknowledgments

The National Science Foundation has supported this work through Grant No. CTS-0335169. C. S. Dutcher gratefully acknowledges support from the National Science Foundation Graduate Research Fellowship and the American Association of University Women Engineering Dissertation Year Fellowship.

References

Andereck, C. D., S. S. Liu and H. L. Swinney, 1986, Flow regimes in a circular couette system with independently rotating cylinders, *J. Fluid Mech.* **164**, 155-183.

Baumert, B.M., and S. J. Muller, 1995, Flow Visualization of the Elastic Taylor-Couette Instability in Boger Fluids, *Rheologica Acta* **34**, 147-159.

Baumert, B.M., S. J. Muller and D. Liepmann, 1997a, Digital particle image velocimetry in flows with nearly closed pathlines: the viscoelastic taylor-couette instability, *J. Non-Newtonian Fluid Mech.* **69**, 221-237.

Baumert, B. M. and S. J. Muller, 1997b, Flow regimes in model viscoelastic fluids in a circular couette system with independently rotating cylinders, *Phys. Fluids* **9**, 566-586.

Baumert, B.M. and S.J. Muller, 1999, Axisymmetric and non-axisymmetric elastic and inertio-elastic instabilities in taylor-couette flow, *J. Non-Newtonian Fluid Mech.* **83**, 33-69.

Cole, J. A., 1976, Taylor-vortex instability and annulus-length effects, *J. Fluid Mech.* **75**, 1-15.

Coles, D., 1965, Transition in circular couette flow, *J. Fluid Mech.* **21**, 385-425.

Coles, D., 1967, A note on Taylor instability in circular couette flow, *J. Appl. Mech.* **34**, 529-532.

Crumeyrolle, O., I. Mutabazi and M. Grisel, 2002, Experimental study of inertioelastic Couette-Taylor instability modes in dilute and semidilute polymer solutions, *Phys. Fluids* **14**, 1681 -1688.

Denn, M.M. and J. J. Roisman, 1969, Rotational stability and measurement of normal stress functions in dilute polymer solutions, *AIChE J.* **15**, 454 -459.

Di Prima, R.C. and H.L. Swinney, 1985, Instabilities and transition in flow between concentric rotating cylinders, *in Hydrodynamic Instabilities and the Transition to Turbulence, 2nd ed.*, H.L. Swinney and J.P. Gollub, editors, Springer-Verlag, Berlin.

Dutcher, C. S., 2009, Experimental investigations into the transitions to turbulence in newtonian and drag-reducing polymeric taylor-couette flows, Ph.D. Dissertation, University of California, Berkeley.

Dutcher, C. S. and S.J. Muller, 2007, Explicit analytic formulas for newtonian taylor-couette primary instabilities, *Phys. Rev. E* **75**, 047301.

Dutcher, C. S. and S.J. Muller, 2009a, Spatio-temporal mode dynamics and higher order transitions in high aspect ratio Newtonian Taylor-Couette flows, *J. Fluid Mech.* **641**, 85-113.

Dutcher, C. S. and S.J. Muller, 2009b, Effects of low elasticity on the stability of high Reynolds number co- and counter-rotating Taylor-Couette flows, *in preparation.*

Esser, A. and S. Grossmann, 1996, Analytic expression for taylor-couette stability boundary, *Phys. Fluids.* **8**, 1814-1819.

Giesekus, H., 1966, Zur stabilität von strömungen viskoelastischer flüssigkeiten: 1. ebene und kreisförmige couetteströmung, *Rheol. Acta* **5**, 239-252.

Giesekus, H., 1972, On instabilities in poiseuille and couette flows of viscoelastic fluids, in *Progress in Heat and Mass Transfer,* **5**, ed. W. R. Schowalter, A. V. Luikov, W. J. Minkowycz, and N.H. Afgan, Permagon, NY, pp. 187-193.

Ginn, R.F. and M.M. Denn, 1969, Rotational stability in viscoelastic liquids: theory, *AIChE Journal* **15**, 450-454.

Groisman, A. and V. Steinberg, 1996, Couette-Taylor flow in a dilute polymer solution, *Phys. Rev. Lett.* **77**, 1480-1483.

Groisman, A., and V. Steinberg, 1997, Solitary vortex pairs in viscoelastic couette flow, *Phys. Rev. Lett* **78**, 1460-1463.

Groisman, A., and V. Steinberg, 1998, Mechanism of elastic instability in couette flow of polymer solutions: experiment, *Phys Fluids* **10**, 2451-2463.

Haas, R. and K. Bühler, 1989, Einfluß nichtnewtonsher stoffeigenschaften auf die taylor-wirbelströmung, *Rheol Acta* **28**, 402-413.

Koschmieder, E. L., 1993, *Bénard cells and Taylor vortices*, Cambridge University Press, Cambridge.

Larson, R.G., 1992, Instabilities in viscoelastic flows, *Rheologica Acta* **31**, 213-263.

Muller, S.J., 2008, Elastically-influenced instabilities in Taylor-Couette and other flows with curved streamlines: a review, *Korea-Australia Rheology J.* **20**, 117-125.

Petrie, C.J.S. and M.M. Denn, 1976, Instabilities in polymer processing, *AIChE J.* **22**, 209-236.

Rubin, H. and C. Elata, 1966, Stability of couette flow of dilute polymer solutions, *Phys. Fluids* **9**, 1929-1933.

Shaqfeh, E.S.G., 1996, Purely elastic instabilities in viscometric flows, *Annual Rev. Fluid Mech.*, **28**, 129-185.

Tagg, R., 1994, The couette–taylor problem, *Nonlinear Sci. Today* **4**, 2-25.

Thomas, D.G., B. Khomami and R. Sureshkumar, 2009, Nonlinear dynamics of viscoelastic taylor-couette flow: effect of elasticity on pattern selection, molecular conformation, and drag, *J. Fluid Mech.* **620**, 353-382.

Thomas, D.G., R. Sureshkumar, and B. Khomami, 2006, Pattern formation in taylor-couette flow of dilute polymer solutions: dynamical simulations and mechanism, *Phys. Rev. Lett.* **97**,

054501.

Thomas, D.G., U.A. Al-Mubaiyedh, R. Sureshkumar and B. Khomami, 2006, Time-dependent simulations of non-axisymmetric patterns in taylor-couette flow of dilute polymer solutions, *J. Non-Newtonian Fluid Mech.* **138**, 111-133.

Walden, R. W. and R.J. Donnelly, 1979, Reemergent order of chaotic circular Couette flow, *Phys. Rev. Lett.* **42**, 301-304.

White, J.M., 2002, *Experimental Investigation of Instabilities in Newtonian and Viscoelastic Taylor-Couette Flows*, Ph.D. Dissertation, University of California, Berkeley.

White, J.M. and S.J. Muller, 2002a, Experimental studies on the stability of newtonian taylor-couette flow in the presence of viscous heating, *J. Fluid Mech.* **462**, 133-159.

White, J.M. and S.J. Muller, 2002b, The role of thermal sensitivity of fluid properties, centrifugal destabilization, and nonlinear disturbances on the viscous heating instability in newtonian taylor-couette flow, *Phys. Fluids* **14**, 3880-3890.

White, J.M. and S.J. Muller, 2003, Experimental studies on the effect of viscous heating on the hydrodynamic stability of viscoelastic taylor-couette flow, *J. Rheol.* **47**, 1467-1492.

Yi, M.K. and C. Kim, 1997, Experimental studies on the taylor instability of dilute polymer solutions, *J. Non-Newtonian Fluid Mech.* **72**, 113-139.